Journal of Atmospheric and Terrestrial Physics, Vol. 41, pp. 527–541

0021-9169/79/0501-0527$02.00/0

Comparisons between various semi-empirical thermospheric models of the terrestrial atmosphere

F. BARLIER, C. BERGER and J. L. FALIN

Centre d'Etudes et de Recherches Géodynamiques et Astronomiques, 8 Boulevard Emile-Zola, F-06130 Grasse, France

G. KOCKARTS

Institut d'Aéronomie Spatiale de Belgique, 3 Avenue Circulaire, B-1180 Bruxelles, Belgique

and

G. THUILLIER

Service d'Aéronomie du CNRS, Boîte Postale no. 3, F-91370 Verrieres-le-Buisson, France

(*Received* 25 *September* 1978; *in revised form* 21 *November* 1978)

Abstract—The availability of various global thermospheric models allows intercomparisons to be made for identical geophysical conditions. Solar activity effect, geomagnetic effect, diurnal variation, annual variation and latitudinal–seasonal dependence are analyzed in four semi-empirical models, viz. DTM, MSIS, ESRO 4 and J77. Emphasis is given to the discrepancies between the models, and some direct comparisons are made with satellite drag data and micro-accelerometer results. None of the semi-empirical models can represent correctly *all* geophysical aspects of the terrestrial thermosphere.

1. INTRODUCTION

The availability of large data bases resulting from *in situ* measurements of various thermospheric parameters has led to the development of a new generation of three-dimensional models of the terrestrial upper atmosphere (HEDIN *et al.*, 1977a, b; VON ZAHN *et al.*, 1977; JACCHIA, 1977). In order to construct any model, it is necessary to determine the thermopause temperature which is usually inferred from composition or total density measurements. However, optical measurements of the width of 630 nm line of atomic oxygen provided a unique opportunity to construct a global temperature model (THUILLIER *et al.*, 1977a) independently of any assumption related to the distribution of atmospheric constituents. This model has recently been combined with satellite drag data to construct a new three-dimensional thermospheric model (BARLIER *et al.*, 1978b) which we shall represent by the acronym DTM (Drag Temperature Model). The purpose of the present paper is to compare DTM with other recent thermospheric models. After a brief summary of the basic principles involved in the construction of DTM, the known geophysical variations of the upper atmosphere are compared in the presently available models. Although general agreement is usually obtained between the various models, specific discrepancies still warrant further investigations.

2. THE DRAG TEMPERATURE MODEL (DTM)

Since satellite drag data lead to total density in the vicinity of the perigee, some assumptions must be introduced to obtain concentrations for each atmospheric constituent. The construction of DTM is based on the fact that molecular nitrogen, atomic oxygen and helium are successively the major atmospheric constituents above 120 km as a consequence of diffusion separation in the Earth's gravitational field. With a mathematical formalism similar to the approach introduced for the first time by HEDIN *et al.* (1974) in thermospheric modeling, BARLIER *et al.* (1978b) used an iterative procedure to represent the three major constituents N_2, O and He in terms of spherical harmonics at 120 km altitude. Using the thermopause temperature model of THUILLIER *et al.* (1977a) and an analytical temperature profile (WALKER, 1965) it is then possible to compute concentrations for the major atmospheric constituents at a given altitude as a function of local solar time, latitude, day number in the year, solar decimetric flux and geomagnetic index K_p. The detailed formalism as well as a computer program are given by BARLIER *et al.*

(1978b) who discussed also several geophysical features of DTM.

Although the distribution of molecular oxygen can be deduced from DTM, it is not given in terms of spherical harmonics since, above 120 km, O_2 is never a major constituent which could account for more than 50% of the total density. DTM gives an O_2 distribution in diffusive equilibrium with a constant lower boundary value at 120 km. A similar remark applies to argon. Atomic hydrogen becomes a major constituent above 1000 km for low solar activity (KOCKARTS and NICOLET, 1963). There are unfortunately not enough satellite drag data in this height region to allow the construction of a reliable model for H over a wide range of geophysical conditions. In consequence, our comparisons with other models will be restricted to temperature, total density, and the concentrations of N_2, O and He.

As an example, Fig. 1 shows a comparison between total densities ρ_{DTM}, computed with DTM, and observed densities ρ_{OBS} deduced from drag data from Cosmos Rocket 1965-11D. The latitude and altitude of satellite perigee indicate to which location in the atmosphere correspond ρ_{DTM} and ρ_{OBS}. Solar activity and geomagnetic activity levels are characterized, respectively, by the daily solar decimetric flux F(in 10^{-22} W m^{-2} Hz^{-1}) and the K_p index for the corresponding period. It appears that a reasonable agreement is reached between the DTM and the observed densities, although the latter represent only a small fraction of the 36,000 total densities effectively used for constructing DTM. Not all the values ρ_{OBS} shown in Fig. 1 have been used in DTM, since the perigee altitude of Cosmos Rocket 1965-11D is in a height range where atomic oxygen progressively becomes more important than molecular nitrogen. Observed densities effectively used for constructing DTM were selected in such a way that atomic oxygen represents 70% of the total density, or that molecular nitrogen leads to 50% of the total density (BARLIER *et al.*, 1978b). Therefore, the agreement between ρ_{OBS} and ρ_{DMT} in Fig. 1 is not only an *a*

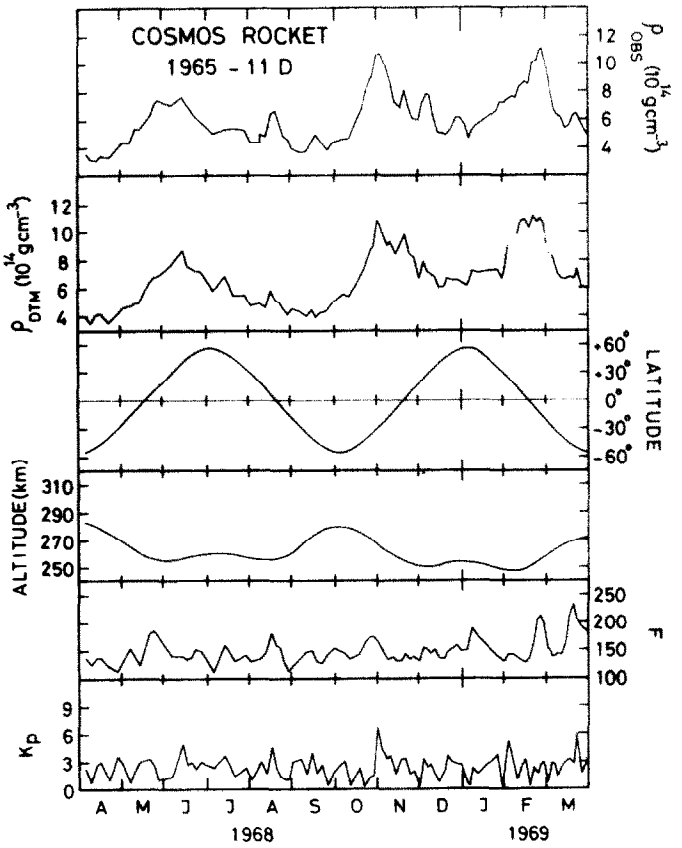

Fig. 1. Comparison of total densities ρ_{OBS} deduced from drag data of Cosmos Rocket 1965-11D and model densities ρ_{DTM}. Latitude and altitude of satellite perigee are given from April 1968 through March 1969. Daily solar decimetric flux F in 10^{-22} W m^{-2} Hz^{-1} and geomagnetic index K_p.

posteriori check of a numerical fitting procedure, but it also reflects the degree of capability to reproduce observed total densities. Other comparisons with drag data will be made in Section 4.

3. COMPARISON WITH OTHER MODELS

DTM will essentially be compared with three other semi-empirical models, viz. MSIS, ESRO4 and J77. The mass spectrometer incoherent scatter model MSIS (HEDIN *et al.*, 1977a, b) is constructed with data gathered from 1966 to 1976 when the mean solar decimetric flux F varied between 70×10^{-22} W m^{-2} Hz^{-1} and 180×10^{-22} W m^{-2} Hz^{-1}. The ESRO4 model (VON ZAHN *et al.*, 1977) is based on mass spectrometer data obtained between December 1972 and April 1974 when the mean solar decimetric flux was between 65×10^{-22} W m^{-2} Hz^{-1} and 145×10^{-22} W m^{-2} Hz^{-1}. The J77 model (JACCHIA, 1977) is constructed with satellite drag data extending from 1958 to 1975: hence this model, as well as DTM (BARLIER *et al.*, 1978b) covers almost two solar cycles. It should be noted, however, that the temperature model (THUILLIER *et al.*, 1977a) used in DTM is based on data obtained only between 8 June 1969 and 16 August 1970. During this period the daily solar decimetric flux F varied between 103 and 239×10^{-22} W m^{-2} Hz^{-1} and the mean solar flux $\bar{F}$ ranged from 136 to 170×10^{-22} W m^{-2} Hz^{-1}. In the following comparisons we refer essentially to two solar activity levels, viz. $\bar{F}=150\times10^{-22}$ W m^{-2} Hz^{-1} (high solar activity) and $\bar{F}=92\times10^{-22}$ W m^{-2} Hz^{-1} (low solar activity for ESRO 4 period).

Although the models discussed in the present paper are constructed using different data covering different time periods and geographic areas, comparisons have to be made under identical conditions. The ESRO4 model will, therefore, sometimes be used for geophysical conditions which have almost never been encountered by the satellite ESRO4, 1972-92A. Similar situations can also occur for the other models.

3.1 *Solar activity effect*

In all semi-empirical models, solar activity is taken into account by relations involving the daily 10.7 cm flux F and some mean value $\bar{F}$ computed over several solar rotations. The solar activity effect, can therefore, be investigated by computing daily averaged quantities as a function of the mean solar decimetric flux. Figure 2 shows daily averaged thermopause temperature, total density and partial concentrations computed on 21 September at the geographic equator for an altitude of 400 km. Daily averaged quantities have been obtained by assuming the daily 10.7 cm flux equal to the mean solar

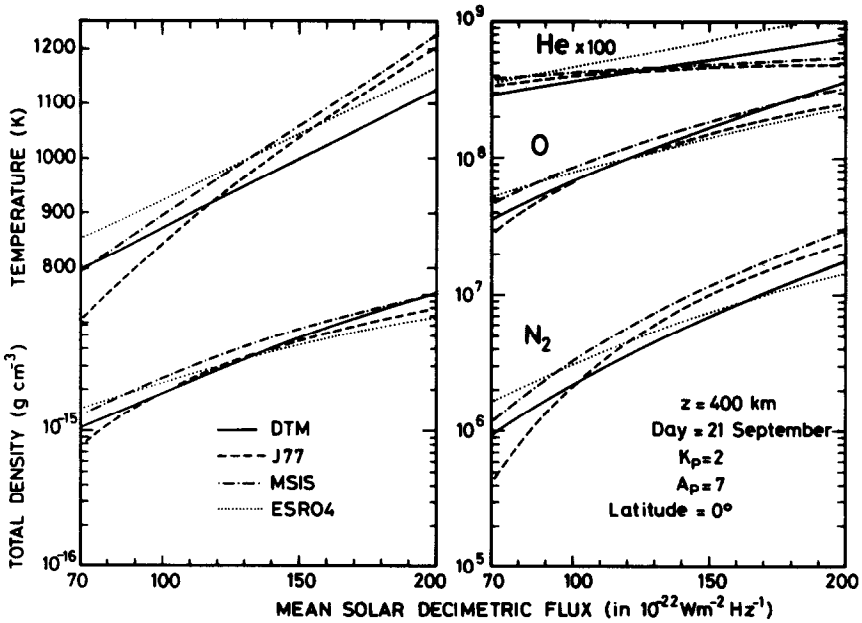

Fig. 2. Daily averaged thermopause temperature, total density and partial concentrations at the equator as a function of mean solar decimetric flux. Comparison at 400 km between DTM, J77, MSIS and ESRO4 on 21 September for $K_p=2$ or $A_p=7$.

decimetric flux, and by adopting constant geomagnetic indices $K_p = 2$ or $A_p = 7$.

As a general rule, the best agreement between the models is obtained for mean solar decimetric fluxes ranging from approximately 100×10^{-22} W m^{-2} Hz^{-1} to 150×10^{-22} W m^{-2} Hz^{-1}. The largest discrepancies occur for very low and very high fluxes as a probable consequence of the smaller amount of data available for extreme geophysical conditions. One should, therefore, realize that temperature differences of the order of 100 K and total density ratios of almost a factor of two can be obtained with the various models under extreme conditions. These differences are also reflected in the partial concentrations. At 400 km the largest differences are seen for N_2 which is a minor constituent at this altitude. It is evident, however, from Fig. 2 that J77, MSIS, ESRO4 and DTM roughly show a similar solar activity dependence with some noticeable differences depending on the solar activity level.

Perfect agreement between a model and a specific experimental result should not be used at the present time as proof of the complete validity of the model for all geophysical conditions. For instance ESRO4 model is constructed with data corresponding to rather low solar activity (average $\bar{F} = 92 \times 10^{-22}$ W m^{-2} Hz^{-1}) and extrapolation to high $\bar{F}$ values should be made with caution.

3.2 *Geomagnetic effect*

In all the models, variations associated with geomagnetic activity are expressed in terms of planetary K_p or A_p indices. Such indices are used in the spherical harmonic expansions for temperature and partial concentrations in DTM, MSIS and ESRO4. The situation is slightly different in J77 where the geomagnetic effect is represented by three terms. According to JACCHIA *et al.* (1977) the local increase in the thermopause temperature is a function of magnetic latitude and is accompanied by a variation in the height of the homopause. The geomagnetic perturbation propagates from high to low latitudes and causes an increase in the total density in the equatorial region a few hours later. The introduction of magnetic latitude is responsible of a longitudinal effect as shown in Fig. 3 where the temperature increase for $K_p = 6$ is represented in a geographic coordinate system. Computations are made for a centered-dipole geomagnetic field. Since spherical harmonic models assume an equivalence between geographic longitude and local solar time, it is necessary to specify, in J77, the geographic longitude when comparisons are made with the other models.

Figure 4 compares the geomagnetic effect in the various models, for equinox conditions (21 September) at 400 km altitude as a function of geographic latitude. The results presented in Fig. 4 are obtained in the following way: each quantity has been daily averaged at 400 km for $K_p = 0$ ($A_p = 0$) and for $K_p = 5$ ($A_p = 48$), then ratios 'disturbed'/'quiet' are computed for concentrations and total density whereas diurnally averaged temperature differences are plotted as a function of geographic latitude. All quantities are computed

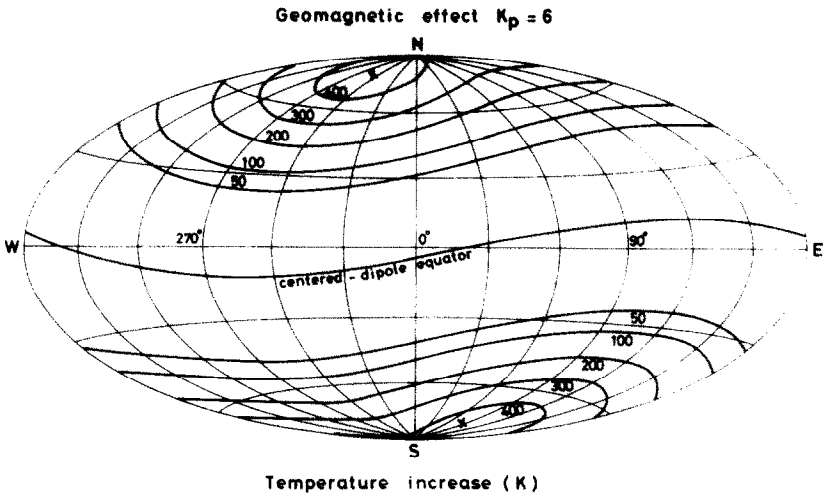

Fig. 3. Global distribution of the temperature increase (K) for $K_p = 6$ in a geographic coordinate system for J77 model.

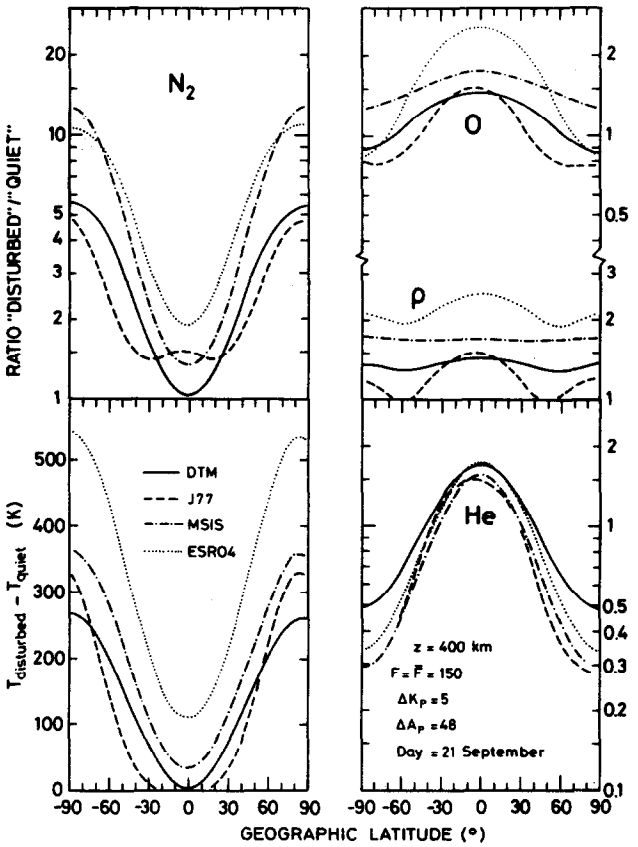

Fig. 4. Geomagnetic effect for $\Delta K_p = 5(\Delta A_p = 48)$ on temperature, partial concentrations (N_2, O, He) and total density ρ at 400 km on 21 September for solar decimetric fluxes $F = \bar{F} = 150 \times 10^{-22}$ W m^{-2} Hz^{-1}. For J77 longitude is 0°.

for $F = \bar{F} = 150 \times 10^{-22}$ W m^{-2} Hz^{-1} and J77 model is used with a geographic longitude of zero degree.

All the models are characterized by similar trends although noticeable differences in amplitude are observed. Temperature and molecular nitrogen concentrations systematically increase towards polar regions, whereas helium decreases in the polar regions for an increase of geomagnetic activity. The decrease of atomic oxygen at the poles is less pronounced at 400 km and this constituent starts moreover to increase towards the poles at higher altitudes. Such features are consistent with a theoretical analysis of magnetic storms (Mayr and Volland, 1973). The small latitudinal variation of the total density ρ at 400 km, with its weak minima around ±45°, results from the combined effect of O and He variations. Since there is no variation of the N_2 homopause with geomagnetic activity, the small equatorial maximum of N_2 in J77 is a consequence of the 'equatorial wave' (Jacchia *et al.*, 1977) which affects all atmospheric constituents by the same amount.

Since the thermospheric energy input responsible for the geomagnetic effect is linked to the auroral oval in such a way that contractions and expansions of the oval lead to variations in the geographical extent of the heating zone (Banks, 1977), it is clear that changes in chemical composition should depend not only on geographic latitude, but also on longitude and local solar time. Realistic comparisons are, therefore, difficult in the polar regions since they depend very much on the time and geographic distributions of the data used in the various models. As a consequence, it is not surprising that the largest discrepancies between the models occur near the poles.

3.3 *Diurnal variation*

When a semi-empirical model is constructed with constant values at the lower boundary above which

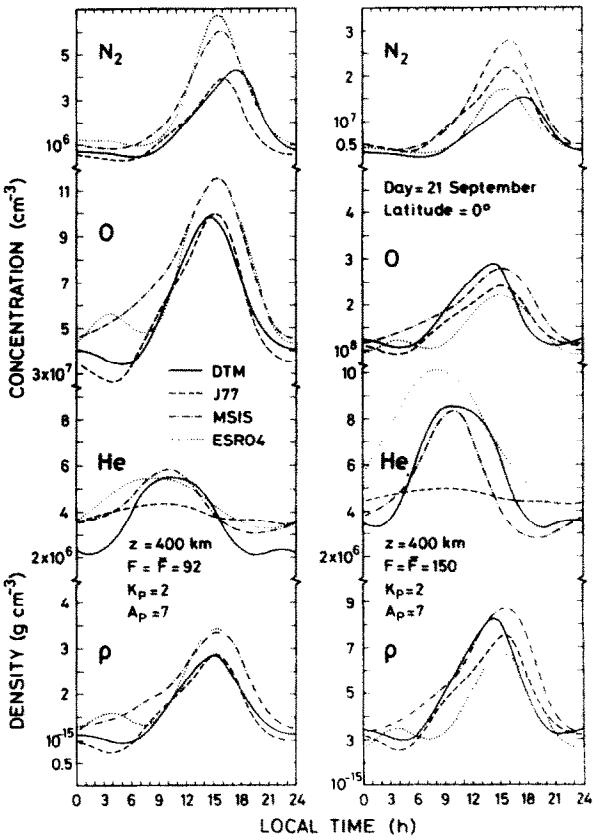

Fig. 5. Diurnal variation of N_2, O, He and total density at the equator on 21 September. Altitude = 400 km. Two solar activity levels $F = \bar{F} = 92 \times 10^{-22}\,\mathrm{W\,m^{-2}\,Hz^{-1}}$ and $F = \bar{F} = 150 \times 10^{-22}\,\mathrm{W\,m^{-2}\,Hz^{-1}}$. Geomagnetic index $K_p = 2$ or $A_p = 7$. For J77 longitude is 0°.

diffusive equilibrium is assumed, partial concentrations and total density are in phase with temperature at altitudes above the isopycnic level, viz. above approximately 150 km for a lower boundary around 120 km. For various reasons, this situation does not occur for any of the models under discussion. The J77 model starts at 90 km with constant boundary values, but it allows empirical corrections between 90 km and 120 km to simulate departures from diffusive equilibrium. At 120 km the spherical harmonic models DTM and ESRO4 adopt variable concentrations resulting from a spherical harmonic analysis performed on data obtained at higher altitude. In MSIS, concentrations at 120 km are also variable, but the shape parameter of the vertical temperature profile is given in terms of spherical harmonics. Furthermore the magnetic term and the diurnal terms for O, He and Ar are multiplied by an empirical function which is intended to represent high magnetic activities and departures from diffusive equilibrium (HEDIN *et al.*, 1977b). For these reasons, all models lead, at high altitude, to diurnal maxima occurring at different times for the different species.

Figure 5 shows diurnal variations at the equator on 21 September for low ($F = \bar{F} = 92 \times 10^{-22}\,\mathrm{W\,m^{-2}\,Hz^{-1}}$) and high ($F = \bar{F} = 150 \times 10^{-22}\,\mathrm{W\,m^{-2}\,Hz^{-1}}$) solar activity at 400 km altitude. It can be seen that the helium maximum occurs always in the morning, followed in sequence by the atomic oxygen and the molecular nitrogen maxima. Total density ρ peaks around 1500 h local solar time. Using a linear theory, MAYR and HARRIS (1977) explained these features in terms of thermal expansion and wind-induced diffusion. Although the phases given by the models agree roughly with theory above 200 km, larger discrepancies occur below that height where unfortunately far fewer experimental data are available. The situation is even worse with regard to the amplitude of the diurnal variation. For instance, ESRO4 shows a secondary maximum in atomic oxygen and total

density, whereas a very small diurnal variation of He is seen in J77.

An interesting comparison can be made for atomic oxygen since this constituent can be deduced from data obtained at the French incoherent scatter facility at Saint-Santin (44.6° N). Although the incoherent scatter technique yields measurements of the electron density and of the electron and ion temperatures at a given altitude and at a given time, BAUER *et al.* (1970) have shown that the neutral atomic oxygen concentration and the neutral thermopause temperature can be deduced from these measurements. The method is based on a balance between the thermal loss from electrons to ions and the thermal loss from ions to neutrals at altitudes ranging from 220 to 500 km. A simultaneous determination of atomic oxygen and the neutral temperature is possible only for daytime conditions when the electron and ion temperatures are different. During the night the incoherent scatter data in the F-region lead only to the neutral temperature which is then equal to the ion and electron temperatures. The validity of such an approach has been reanalyzed in great detail by ALCAYDÉ and BAUER (1977). Comparisons with various models for long term variations of atomic oxygen and of thermopause temperature have been made recently by ALCAYDÉ *et al.* (1978). Generally good agreement has been found for the long term variations at 45° N. The incoherent scatter results will not be discussed, therefore, in the following sections dealing with long term variations. We refer the interested reader to the work of ALCAYDÉ *et al.* (1978).

Up to now no systematic comparison of the diurnal variation of atomic oxygen deduced from incoherent scatter data and values resulting from the presently discussed semi-empirical models is available. Figure 6 shows, therefore, the diurnal variation at 400 km for equinox and solstice condi-

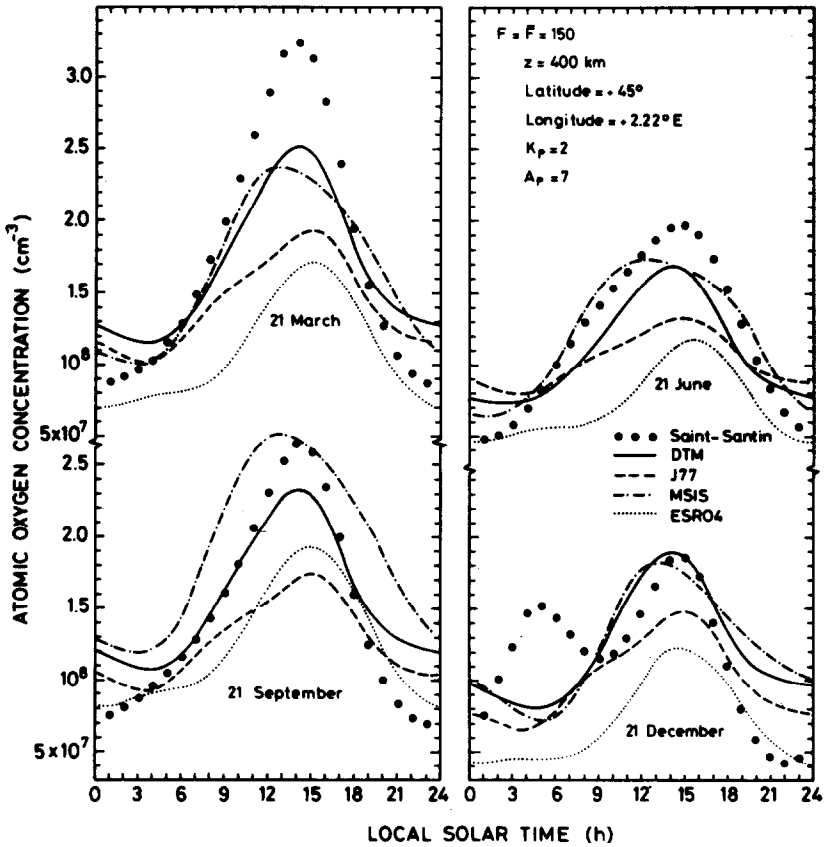

Fig. 6. Comparison of atomic oxygen incoherent scatter model above Saint-Santin (ALCAYDÉ and BAUER, 1977) with J77, MSIS, ESRO4 and DTM for equinox and solstice conditions. Solar activity level $F = \bar{F} = 150 \times 10^{-22}$ W m^{-2} Hz^{-1}. Geomagnetic index $K_p = 2$ or $A_p = 7$. For J77 longitude is 2.22° E, i.e. longitude of Saint-Santin.

tions assuming $F = \bar{F} = 150 \times 10^{-22}$ W m^{-2} Hz^{-1} and $K_p = 2$ or $A_p = 7$. The semi-empirical models discussed in the present paper are compared with the Saint-Santin model deduced by ALCAYDÉ and BAUER (1977). The Saint-Santin model presents the largest amplitude for spring conditions. Furthermore, the afternoon decrease of atomic oxygen is always steeper in the incoherent scatter model. ESRO4 results are also shown in Fig. 6, although this model should probably not be applied for high mean solar decimetric fluxes. In ESRO4, the secondary maximum present at the equator on 21 September (see Fig. 5) is insignificant at 45° N (see Fig. 6). It is difficult to say, at present, whether such a feature is real. A similar remark is valid for the secondary maximum given by the Saint-Santin model on 21 December, since this model is based on data obtained during daytime. All the nighttime values in the Saint-Santin model actually result from extrapolations. Despite this fact it could be useful to introduce atomic oxygen incoherent scatter data in the semi-empirical thermospheric models.

From the comparisons made in this section, it appears that the diurnal variation is probably the less well represented phenomenon in all global thermospheric models. This is not surprising since, at a specific location, it is usually difficult with satellites to get a good data coverage in local time for a given set of geophysical parameters.

3.4 *Annual variation of diurnally averaged thermopause temperature and molecular nitrogen concentration at ±45° latitude*

Another important variation in the upper atmosphere is the annual variation related to changes in illumination according to the position of the Earth on its orbit around the sun. We shall first examine the annual variations of the thermopause temperature and molecular nitrogen concentration since these two parameters are characterized by a similar behaviour in the course of a year.

All the quantities shown in Figs 7 and 8 are diurnally averaged for two levels of solar activity ($F = \bar{F} = 92 \times 10^{-22}$ W m^{-2} Hz^{-1} and $F = \bar{F} = 150 \times 10^{-22}$ W m^{-2} Hz^{-1}) and for $K_p = 2$ or $A_p = 7$. For J77, the adopted longitude is 2.22°E. Constant solar decimetric flux and constant K_p or A_p indices never prevail for periods as long as a year, but the hypothesis used in Figs 7 and 8 eliminates short term variations which could mask the characteristics of the annual variation. The overall variation is

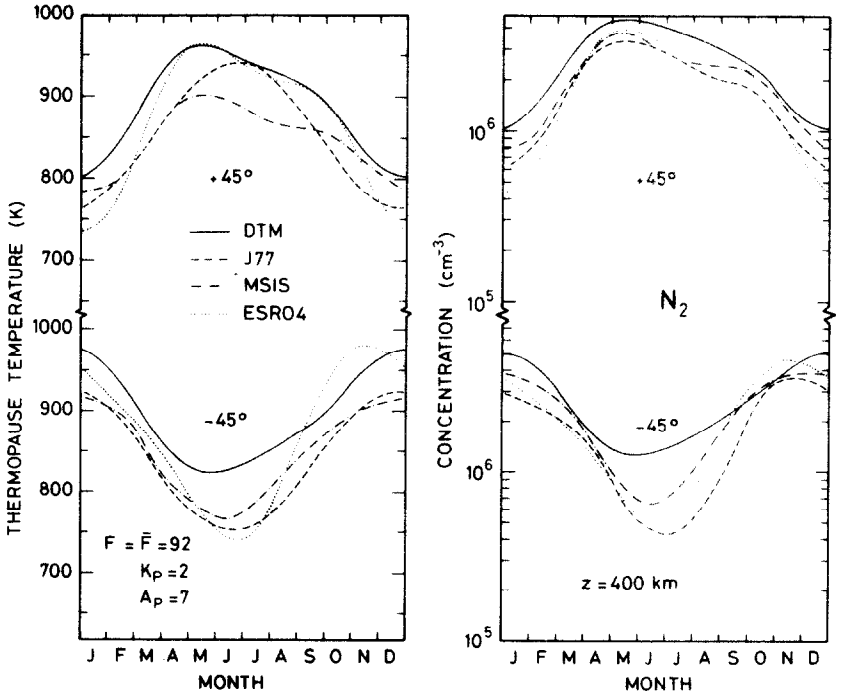

Fig. 7. Diurnally averaged thermopause temperature and molecular nitrogen concentration at 400 km for ±45° latitude. Geomagnetic index $K_p = 2$ or $A_p = 7$. Solar decimetric flux $F = \bar{F} = 92 \times 10^{-22}$ W m^{-2} Hz^{-1}. Longitude 2.22° E for J77.

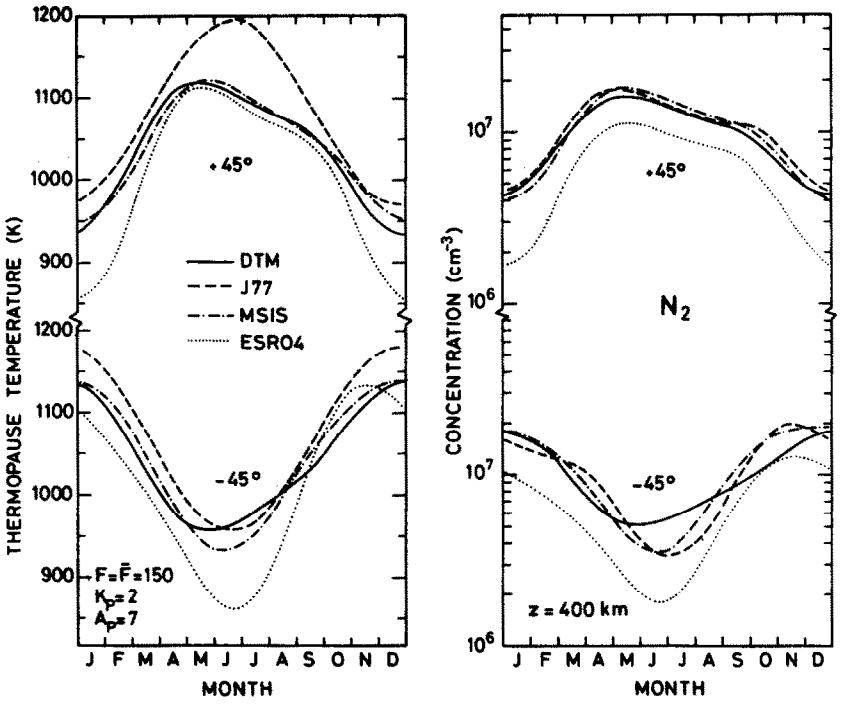

Fig. 8. Same as Fig. 7, but $F = \bar{F} = 150 \times 10^{-22}$ W m^{-2} Hz^{-1}.

dominated by an annual effect whereas the semi-annual effect appears to be small. Marked differences can be seen between the two hemispheres. In the northern hemisphere, the temperature maximum occurs at the end of April (except for J77), whereas in the southern hemisphere the maximum occurs around summer solstice (except for ESRO4). As a general feature the N_2 and temperature variations are significantly different in both hemispheres for all models. In the northern hemisphere the temperature and N_2 decreases are slower after local spring maximum than after local summer in the southern hemisphere. Furthermore, the temperature difference between 45° N and 45° S is higher during December solstice than during June solstice, and the mean temperature around the solstices is higher in the southern hemisphere than in the northern hemisphere at these latitudes. This fact leads to global pressure maps capable of causing, in addition to the normal circulation (Johnson and Gottlieb, 1970), a wind component blowing from south to north. Such characteristics are related to north–south asymmetries discussed by Barlier *et al.* (1974).

The agreement between the various models seems to be better in the northern hemisphere and extrapolation of ESRO4 to high solar fluxes (Fig. 8) does not appear to be valid.

3.5 *Annual variation of diurnally averaged atomic oxygen concentration at ±45° latitude*

The annual variation of atomic oxygen is shown in Fig. 9 at 400 km for both hemispheres and for two solar activity levels. In all the models the variation is dominated by a semi-annual effect characterized by two significant maxima around the equinoxes. Such a behaviour differs completely from what is seen for N_2 (see Figs 7 and 8) and for He (see Fig. 10). At high solar fluxes the minima around January and July are comparable in the northern hemisphere whereas in the southern hemisphere the July minimum is deeper than the summer minimum. In consequence, the variability of atomic oxygen is greater in the southern hemisphere than in the northern hemisphere at 400 km altitude.

For low solar activity the difference between both hemispheres is not so evident although there exists a similar tendency. The minimum during local winter solstice is always deeper than the minimum during local summer solstice, contrary to the situation for high solar activity.

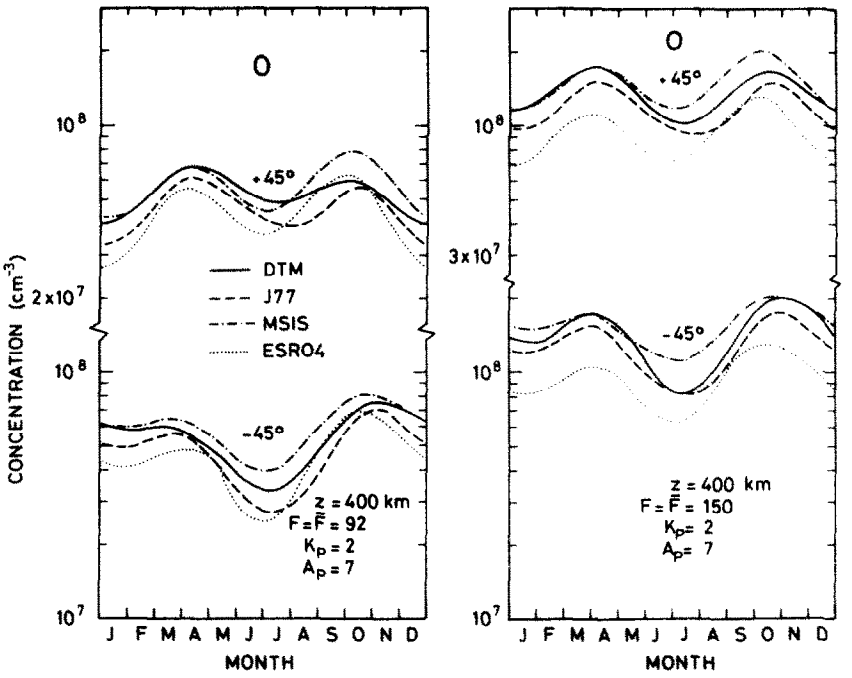

Fig. 9. Diurnally averaged atomic oxygen concentration at 400 km for ±45° latitude. Geophysical conditions identical as in Figs 7 and 8.

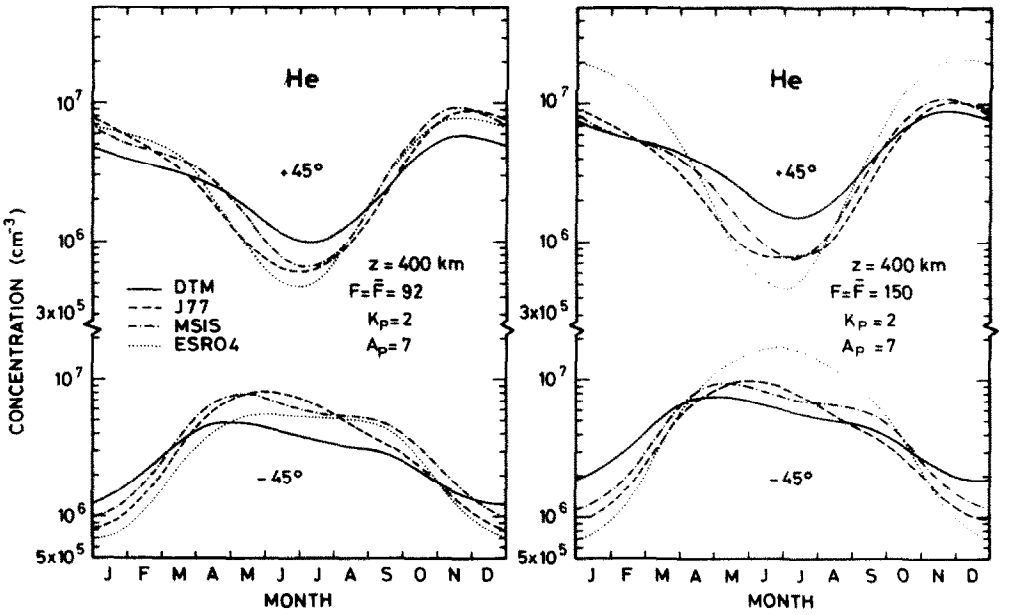

Fig. 10. Diurnally averaged helium concentration at 400 km for ±45° latitude Geophysical conditions identical as in Figs 7 and 8.

Since atomic oxygen is the major constituent at 400 km, the variations shown in Fig. 9 can be related to the classical result of the semi-annual variation of the total density (CIRA, 1972) with an October maximum higher than the April value. From a recent analysis of the orbit of Cosmos 462, 1971-106A, WALKER (1978) concludes, however, that the April value near 200 km is higher than the October value. Such a feature appears also in DTM for low solar activity. However, a more detailed analysis should be made since Fig. 9 indicates different behaviours for different latitudes and solar activity levels.

Finally it should be noted that comparisons of various models with atomic oxygen deduced from incoherent scatter data (ALCAYDÉ *et al.*, 1978) show a reasonable agreement for the annual variation at 400 km. It has been shown in Fig. 6 that a similar conclusion connot be made for the diurnal variation.

3.6 *Annual variation of diurnally averaged helium concentration at ±45° latitude*

The annual variation of helium is shown in Fig. 10 at 400 km for two solar activity levels. The annual variation of helium is in anti-phase with the annual variation of temperature and molecular nitrogen (see Figs 7 and 8). If an imaginary hemispherical reversal is made in Fig. 10, the similarity between the He and N_2 annual variations is very clear. The phase difference of the order of 6 months probably results from large scale transport associated with the helium winter bulge. Furthermore, the helium behavior is similar in both hemispheres. The semi-annual effect is small as for N_2. Finally the seasonal variability is higher in the northern hemisphere.

3.7 *Latitudinal and seasonal variations of helium*

In order to analyze latitudinal and seasonal variations of helium, diurnally averaged concentrations are computed at 1000 km for winter and summer solstices. The results obtained for various models are shown in Fig. 11, for two solar acticity levels, as a function of geographic latitude. The winter helium bulge is clearly present in all models although the winter to summer ratios vary greatly from one model to another, especially in the polar regions. At a given pole the discrepancy between the models is larger during local summer, i.e. when the helium concentration is small. During local summer in the polar regions, models based on mass spectrometer data always give lower values than DTM, which is entirely based on drag data. This fact can be related to the difficulty of measuring low helium abundances by mass spectrometry

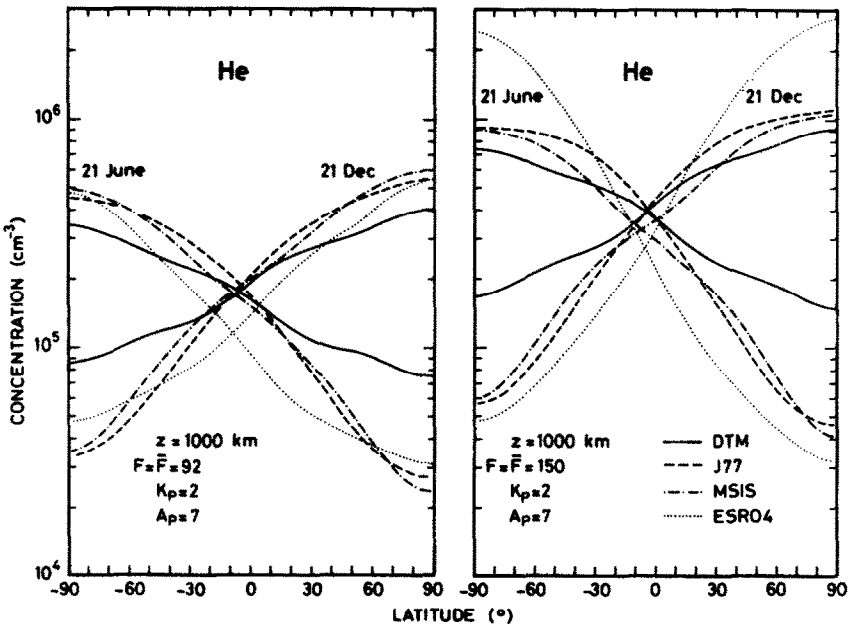

Fig. 11. Latitudinal variation of diurnally averaged helium concentration at 1000 km for two solar activity levels ($F = \bar{F} = 92 \times 10^{-22}$ W m^{-2} Hz^{-1} and $F = \bar{F} = 150 \times 10^{-22}$ W m^{-2} Hz^{-1}) and for $K_p = 2$ or $A_p = 7$. Longitude 2.22° E for J77.

(TRINKS *et al.*, 1977). Furthermore, model comparisons in the polar regions are perhaps not very realistic since a large longitudinal effect could have been omitted in all models. In any case, the large discrepancy between drag data and mass spectrometric data for very low helium abundances remains an unsolved problem at the present time.

4. COMPARISON BETWEEN SPECIFIC DRAG DATA AND MODELS

Since the concentrations given by DTM are entirely based on drag data, it is interesting to make comparisons between total densities ρ_{OBS} deduced from drag data, and total densities ρ_{MODEL} computed with the model. Figure 12 shows such comparisons for three satellites. A general agreement can be seen although the ratio ρ_{OBS}/ρ_{MODEL} can be sometimes greater than two, as in 1968 for OV3-2 fragment 1966-97D.

In the same figure we have also plotted the total densities obtained from MSIS, i.e. a model which is not based on satellite drag data. For OV3-2 fragment and Transtage 7 it should be noted that both models follow almost exactly the same trend. The perigees of these two satellites are in a height range where N_2 and O are major atmospheric constituents. The situation slightly changes for ECHO 2 1964-04A which has its perigee around 1150 km where helium is an important atmospheric component. It appears in Fig. 12 that, in July 1964 and in January 1965, model densities obtained with MSIS are systematically lower than values deduced from DTM. This effect is clearly seen in Fig. 13 which shows the ratio ρ_{OBS}/ρ_{MODEL} from 28 June 1964 until 15 January 1965. The results obtained with J77 are also given in this figure. On 22 July 1964 the perigee of ECHO 2 was in the northern hemisphere at 75° latitude. On 26 December 1964 the perigee of ECHO 2 was in the southern hemisphere at −75° latitude. On both days the satellite was, therefore, under local summer conditions at rather high latitudes. According to the

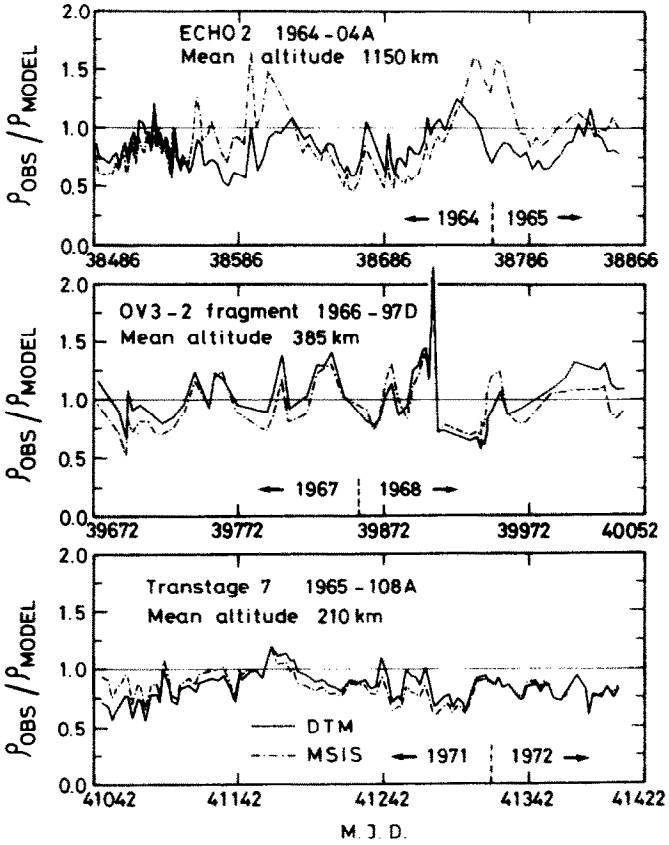

Fig. 12. Ratio ρ_{OBS}/ρ_{MODEL} for three satellites as a function of the modified Julian day (M.J.D.) Model densities are computed, respectively, with DTM and MSIS.

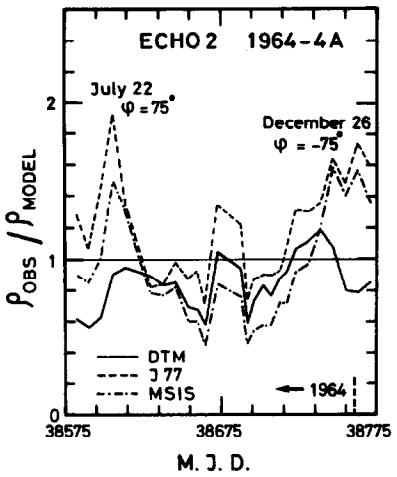

Fig. 13. Ratio ρ_{OBS}/ρ_{MODEL} for ECHO 2 as a function of the modified Julian day (M.J.D.). Model densities are computed, respectively, with DTM, MSIS and J77. Perigee latitude is indicated for 22 July 1964 and 26 December 1964.

characteristics of the winter helium bulge, the drag of ECHO 2 resulted on these 2 days from low helium concentrations. As a consequence the high values of ρ_{OBS}/ρ_{MODEL} for MSIS and J77 imply that the helium concentration is too small in these models for high-latitude summer conditions. It seems that DTM is the only model which appropriately represents the helium summer depression as observed with satellite drag.

The micro-accelerometer CACTUS on board of CASTOR-D5B 1975-39A offers the possibility of comparing high resolution data with model results. The total densities obtained with CACTUS (Barlier *et al.*, 1977, 1978a) have a relative accuracy of 1% between 300 and 400 km altitude. Figure 14 shows a comparison between ρ_{CACTUS} and ρ_{DTM} for five magnetically quiet days during May 1976. Although there is a relatively good agreement between DTM and the micro-accelerometer results, it appears that DTM densities are a little too high. Such a systematic difference could be explained by an overestimation of the thermopause temperature in the optical model of Thuillier *et al.* (1977a) during May 1976. This model agrees, however, with incoherent scatter data obtained in 1966 for low solar activity (Thuillier *et al.*, 1977b). But during the 1966 minimum the mean solar decimetric flux was around $100\times10^{-22}\,W\,m^{-2}\,Hz^{-1}$ whereas in May 1976 it reached values as low as $72\times10^{-22}\,W\,m^{-2}\,Hz^{-1}$. In view of the accuracy of the CACTUS data, the small discrepencies in Fig. 14 cannot be considered as random noise. They show actually an inherent limitation of global

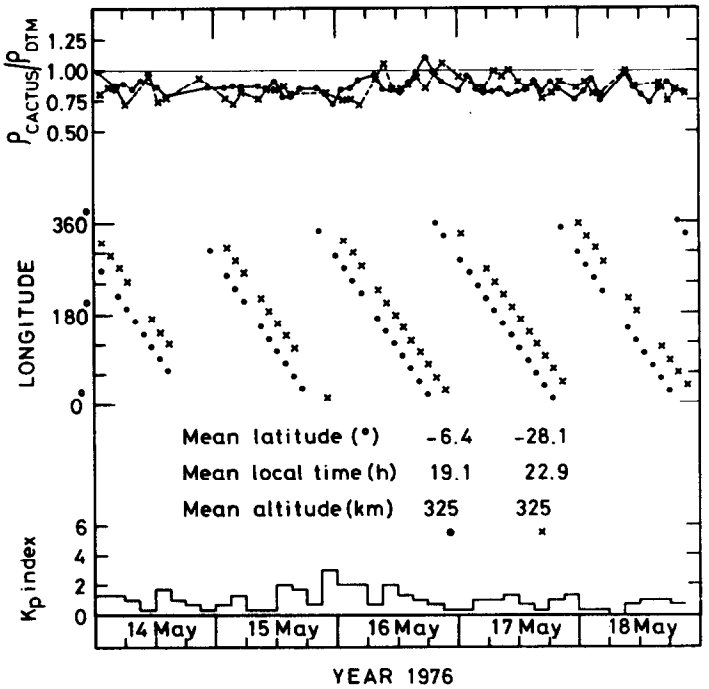

Fig. 14. Comparison between micro-accelerometer densities ρ_{CACTUS} and densities obtained from DTM. Longitude of the satellite is indicated as well as K_p indices.

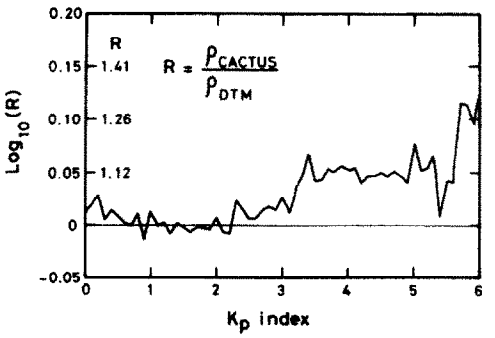

Fig. 15. Comparison between micro-accelerometer densities ρ_{CACTUS} and ρ_{DTM} as a function of geomagnetic index K_p. The CACTUS data are exclusively obtained for low latitudes.

models, namely that they are unable to represent short-term fluctuations in the upper atmosphere.

Finally the CACTUS data show that DTM underestimates the geomagnetic effect for low latitudes and low solar activity. This can be seen from Fig. 15 which represents the decimal logarithm of ρ_{CACTUS}/ρ_{DTM} as a function of the K_p index for almost all the data obtained with the micro-accelerometer. This example indicates that refinements can still be made in global semi-empirical models.

5. CONCLUSION

From the comparisons made in this paper, it would be unfair to conclude that any one of the models is completely inadequate to represent the physical structure of the terrestrial thermosphere. But, it would be pretentious to assert that all the phenomena observed are perfectly well understood and represented.

It is necessary to remember that the solar activity effect is analyzed using data covering at most two solar cycles, and that there can be large differences between different solar cycles. For instance during the very high solar maximum in 1958 only drag data were available, and no *in situ* measurements have ever been performed under such conditions.

The global geomagnetic effect is represented by empirical relations involving K_p or A_p indices deduced from 13 stations which are poorly distributed over the world: 11 stations between 63° N and 50° N geomagnetic latitude and two stations between 46° S and 48° S (IAGA, 1970). It is, therefore, not surprising that some difficulties are encountered at high and low latitudes.

The various models indicate different amplitudes in the diurnal variation of the atmospheric constituents and the phases agree only above 200 km.

For the seasonal–latitudinal variation, a specific problem arises with helium abundance during local summer at high latitude. The large difference between drag data and mass spectrometric data cannot be attributed to geophysical phenomena. It is conceivable that such a problem could be clarified by using extreme ultraviolet optical data for the helium distribution at high altitude.

Except for the geomagnetic effect in J77, in no other model can the mathematical structure account for longitudinal effects as a consequence of the assumed equivalence between longitude and local time. Comparing the ESRO4 data and the ESRO4 model, VON ZAHN and FRICKE (1978) have clearly shown the existence a longitudinal pattern for the atmospheric constituents.

Finally density fluctuations as observed with the micro-accelerometer CACTUS, are far from being well represented by global thermospheric models.

The difficulties encountered with the present semi-empirical models of the terrestrial thermosphere should not be regarded as grounds for criticism of the work carried out in the past, but rather as a stimulation for further research in a field which is only 20 years old.

Acknowledgements—We would like to thank EMILE FALISE (IAS) for his valuable help in the computations required for this work.

REFERENCES

ALCAYDE D. and BAUER P.	1977	*Annls Géophys.* **33,** 305
ALCAYDE D., BAUER, P., HEDIN A. and SALAH J. E.	1978	*J. geophys. Res.* **83,** 1141.
BANKS P. M.	1977	*J. atmos. terr. Phys.* **39,** 179.
BARLIER F., BAUER P., JAECK C., THUILLIER G. and KOCKARTS G.	1974	*J. geophys. Res.* **79,** 5273.
BARLIER F., BOUDON Y., FALIN J. L., FUTAULLY R., VILLAIN J. P., WALCH J. J., MAINGUY A. M. and BORDET J. P.	1977	*Space Res.* **17,** 341.
BARLIER F., BERGER C., BORDET J. P., FALIN J. L., FUTAULLY R. and VILLAIN J. P.	1978a	*Space Res.* **18,** 169.

BARLIER F., BERGER C., FALIN J. L., KOCKARTS G. and THUILLIER G.	1978b	*Annls Géophys.* **34,** 9.
BAUER P., WALDTEUFEL P. and ALCAYDE D.	1970	*J. geophys. Res.* **75,** 4825.
CIRA	1972	*Cospar International Reference Atmosphere.* Akademie, Berlin.
HEDIN A. E., MAYR H. G., REBER C. A., SPENCER N. W. and CARIGNAN G. R.	1974	*J. geophys. Res.* **79,** 215.
HEDIN A. E., SALAH J. E., EVANS J. V., REBER C. A., NEWTON G. P., SPENCER N. W., KAYSER D. C., ALCAYDE D., BAUER P., COGGER L. and MCCLURE J. P.	1977a	*J. geophys. Res.* **82,** 2139.
HEDIN A. E., REBER C. A., NEWTON G. P., SPENCER N. W., BRINTON H. C. and MAYR H. G.	1977b	*J. geophys. Res.* **82,** 2148.
IAGA	1970	Bull. 32. *IUGG* Publications Office, Paris.
JACCHIA L. G.	1977	*Smithson. Astrophys. Obs.*, Spec. Rep. 375.
JACCHIA L. G., SLOWEY J. W. and VON ZAHN U.	1977	*J. geophys. Res.* **82,** 684.
JOHNSON F. S. and GOTTLIEB B.	1970	*Planet. Space Sci.* **18,** 1707.
KOCKARTS G. and NICOLET M.	1963	*Annls Géophys.* **19,** 370.
MAYR H. G. and HARRIS I.	1977	*J. geophys. Res.* **82,** 2628.
MAYR H. G. and VOLLAND H.	1973	*J. geophys. Res.* **78,** 2251.
THUILLIER G., FALIN J. L. and BARLIER F.	1977a	*J. atmos. terr. Phys.* **39,** 1195.
THUILLIER G., FALIN J. L. and WACHTEL C.	1977b	*J. atmos. terr. Phys.* **39,** 399.
TRINKS H., VON ZAHN U., REBER C. A., HEDIN A. E., SPENCER N. W., KRANKOWSKY D., LAMMERZAHL P., KAYSER D. C. and NIER A. O.	1977	*J. geophys. Res.* **82,** 1261.
VON ZAHN U. and FRICKE K. H.	1978	*Rev. Geophys. Space Phys.* **16,** 169.
VON ZAHN U., KOHNLEIN W., FRICKE K. H., LAUX U., TRINKS H. and VOLLAND H.	1977	*Geophys. Res. Lett.* **4,** 33.
WALKER D. M. C.	1978	*Planet. Space Sci.* **26,** 291.
WALKER J. C. G.	1965	*J. atmos. Sci.* **22,** 462.